Impedance Spectra Characteristics of Dy-doped Fe-20Cr Alloys in the Presence of Solid K$_2$SO$_4$-KCl Mixture at 600°C in Air

Y B Lai, P Y Guo*, Y Shao, H Sun, J T Ding, Y X Wan, Y X Qiao and Y X Guo

School of Materials Science and Engineering, Jiangsu University of Science and Technology, Jiangsu 212003, China

Corresponding author and e-mail: P Y Guo, pyguo@just.edu.cn

Abstract. Impedance spectra characteristics of Fe-20Cr, Fe-20Cr-0.2Dy and Fe-20Cr-1Dy alloys are studied in 0.5K$_2$SO$_4$-0.5KCl mixture in air at 600°C. The two-electrode system is used for electrochemical impedance measurements, and it has been proved effective in the study of solid- and molten-salt corrosion. The corrosion of alloys goes through two stages during extended exposure. Impedance spectra of every stage is fitted by an equivalent circuit and corresponding electrochemical elements. The effect of Cr content in Fe-based alloys has been investigated in an attempt to understand corrosion mechanism involving the active/oxidation process of metal Cr. The effect of the additive Dy dissolving and precipitating in Fe-Cr alloy on the hot corrosion has also been investigated. Corrosion products in different stages are analyzed by scanning electron microscopy and the formation and depletion of protective scale in mixed salt is monitored. Corrosion rate and corrosion mechanism of three alloys are discussed.

1. Introduction

KCl-K$_2$SO$_4$ mixture is able to attack the metal surfaces of the superheaters and leads to serious corrosion problems. The development of a material that has a high-corrosion resistance in the combustion deposit containing chloride and sulfate has been advanced[1-3]. High-Cr ferritic and austenitic steels are widely used as high-temperature components and protective chromia scales formed on these alloys surfaces make an immediate impact in corrosion resistance during high-temperature exposure.

In order to improve alloys against high temperature corrosion and extend service life of alloys, some reactive elements can be added in alloys. The rare earth effect is made up of a number of different factors for high temperature corrosion[4-7], such as selective oxidation enhanced, the predominantly transport mechanism altered, void formation suppressed and the adherence of scales increased. The corrosion behavior of Ni-Dy alloys[8,9] showed that a small amount of Dy could retard greatly the corrosion of Ni and the incorporation of Dy into nickel oxide decreased clearly its solubility in molten (Li,K)$_2$CO$_3$ mixture at 650°C. The oxidation of Co-Y and Fe-Y binary alloys at 600-800°C in air[10,11] showed that alloys produced an external scale and a wide internal oxidation region. The rate of oxygen penetration in Co-Y and Fe-Y alloys was faster than in pure cobalt and iron, but outward diffusion cobalt and iron decreased. Oxidation behavior of Dy-doped Fe-20Cr

674

(wt.%) alloys at 900°C in air[12] showed that Dy could significantly improve the oxide resistance of Fe-20Cr. Although a few papers were published on the oxidation behavior of Dy modified alloys, the experiments performed in the solid, partially melted and completely melted KCl-K_2SO_4 mixture for the long exposure time were still interesting.

In this study the high temperature corrosion behavior of Fe-20Cr alloys with the addition of Dy is investigated using simultaneous electrochemical impedance techniques. Test-cell design is important to electrochemical measurements for corrosion of materials. Zeng[13,14] discloses that a two-electrode arrangement comprising two working electrodes can be prepared conveniently, and is also suitable for simple electrochemical impedance measurements.

2. Experimental

Fe-20Cr, Fe-20Cr-0.2Dy and Fe-20Cr-1Dy (wt.%) are employed in the present study. Back-scattered electron images of the annealed alloys are shown in Figure 1. A few white particles are found in Fe-20Cr-0.2Dy, which are Dy-rich precipitates and most are localized at grain boundaries. The solubility of Dy is more lower than 1 wt.% in Fe-20Cr alloys. Fe-20Cr-1Dy are two-phase composed of a Fe solid solution and a Dy-rich phase. Alloy ingots are cut into pieces in the size of 10mm×5mm×1 mm.

The EIS measurements are conducted in the mixed 0.5K_2SO_4-0.5KCl salt (mole fraction) in air at 600°C. The mixed salt is dried at 400°C for 48h and then heated to reaction temperature. During the experiment specimens are totally buried under the mixed salt for about 25mm, and extracted at selected intervals for morphology analysis with the residual potassium salts. A two-electrode system is used for EIS measurements (Figure 1c). The Fe–Cr wire is spot-welded to one end of the specimen for electric connection. Two specimens parallel to each other and are sealed in an alumina tube by a high-temperature cement, with one side uncovered. The high-temperature cement is solidified at 100°C for 24 h and 350°C for 10 h. The size of each working electrode is 5mm×5mm×1mm and they are degreased again for test. The distance of two electrodes is about 1mm to reduce electrolyte resistance between the gap. EIS measurements are performed at open circuit potential between 1×10^{-2} and 1×10^{4} Hz using a computer-controlling high-speed Parstat 2273 of Princeton Applied Research. The amplitude of input sine-wave voltage is 10 mV.
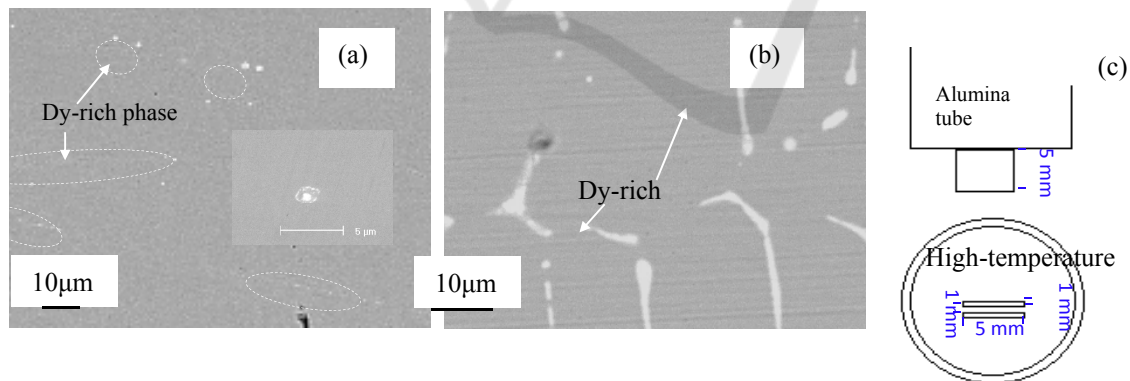

Figure 1. Microstructure of (a) Fe-20Cr-0.2Dy and (b) Fe-20Cr-1Dy alloys (bright phase: Dy-rich phase; dark phase: solid solution), (c) two-electrode system for EIS.

3. Results and discussion

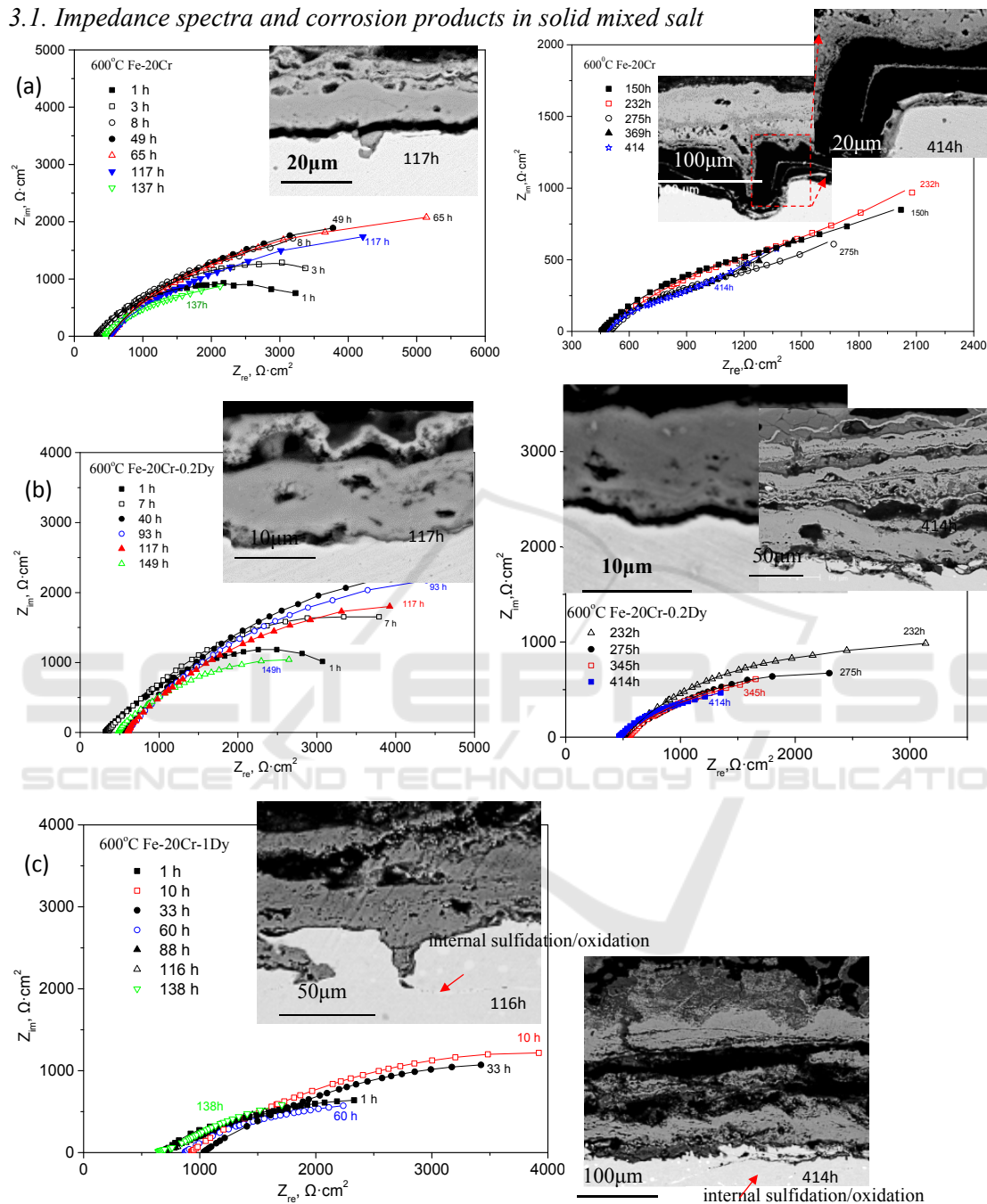### 3.1. Impedance spectra and corrosion products in solid mixed salt

Figure 2. Nyquist plots for alloys buried in K_2SO_4-KCl mixtures at 600°C in air after different exposure times and cross-sectional morphology of alloys after exposure.

Figure 2 shows EIS and cross section of Fe-20Cr corroded in solid mixed salt at 600°C for different time. The Nyquist plots show that it is a large capacitive loop at all frequencies between 1h and 137h, and the diffusion-controlled reaction clearly develops after electrodes corroded for 232h. The external oxides of Fe-20Cr corroded for 117h and 414h are mainly compact Fe/Cr oxides and some

sulfides are found in oxide/metal interface. There is no internal oxidation in Fe-20Cr alloy, but the alloy interface prominently fluctuates after corrosion for 414h.

The Nyquist plots of Fe-20Cr-0.2Dy are composed of a large capacitive loop at all frequencies during the period of 345h, and the modulus of impedance |Z| is obviously larger than Fe-20Cr alloy in initial stage. The Nyquist plots show a line at the low frequency part after corroded for 345h, which means the degradation of protective scale. Oxide products of Fe-20Cr-0.2Dy are mainly Cr-rich oxides and it is thin and compact with a good adhesion to alloy for 117h and 232h. The oxide scale for 414h is composed of an external scale of Fe/Cr oxides plus a mild internal sulfidation/oxidation. Some residual salt is found near to the outermost oxide layer.

The Nyquist plots of Fe-20Cr-1Dy maintain a large capacitive loop at all frequencies during the period of 138 h, however, the modulus of impedance is obviously smaller than that of Fe-20Cr and Fe-20Cr-0.2Dy. Cross section of Fe-20Cr-1Dy shows that the external oxide layer is a little thick. An internal sulfidation/oxidation is observed along the grain boundary in which Dy-rich precipitates are localized. With the extended hours, thick external oxide layer becomes loose and some chlorides are found in the interface of oxide/alloy.

3.2. Corrosion rate

The corrosion rate V_t is proportional to the reciprocal of polarization resistance and the evolution with exposure time is shown in Figure 3. Corrosion rates of three alloys increase with the reaction time. Corrosion rate of Fe-20Cr-1Dy is a little higher than Fe-20Cr and Fe-20Cr-0.2Dy after about 100h. Corrosion rates of Fe-20Cr and Fe-20Cr-0.2Dy in the stage of 100h are almost the same, and then corrosion rate of Fe-20Cr increases and becomes higher than Fe-20Cr-0.2Dy between 100h and 414h. The magnified view shows that corrosion rate of alloys decrease rapidly to a minimum corresponding to about 5h, and then rises gradually, which means the formation of protective scales in the initial stage.
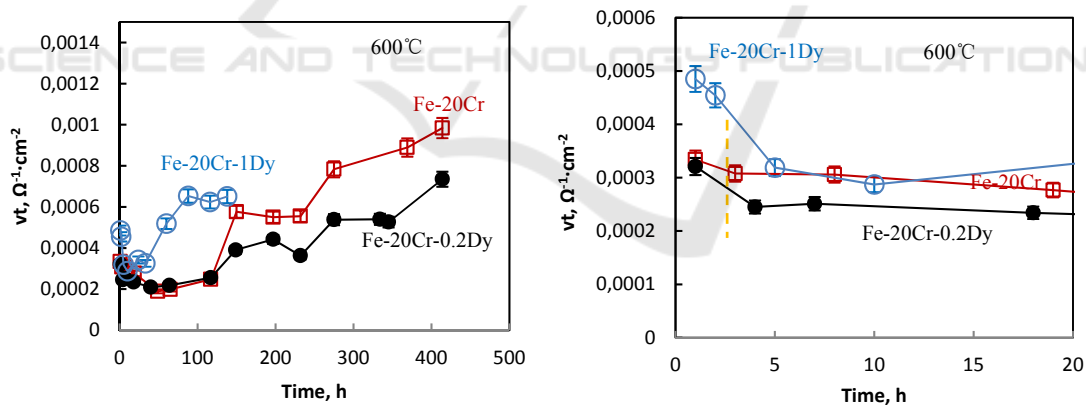

Figure 3. The evolution of corrosion rate with exposure time in mixed salt at three different temperatures.

3.3. Electrochemical impedance models

When alloys corroded at 600°C, reaction temperatures are lower than the melt point of mixed salt. So kali salt on the top of alloys is still solid in the initial stage. Electrochemical impedance spectroscopy is assumed to be only the response of oxide scales forming on the surface. An equivalent circuit of oxide capacitance parallel with scale resistance can be used to represent the single capacitive loop for the corrosion (Figure 4a). With reaction time increasing, mixed kali salt between two electrodes is sintered and may be the semi-melting status. The impedance of a diffusion-controlled reaction can be represented by the equivalent circuit (Figure 4b).
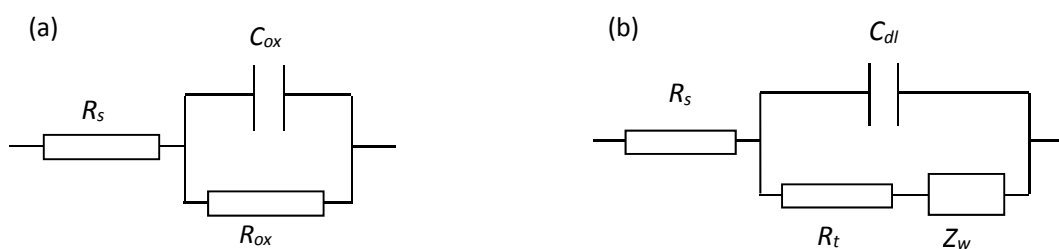
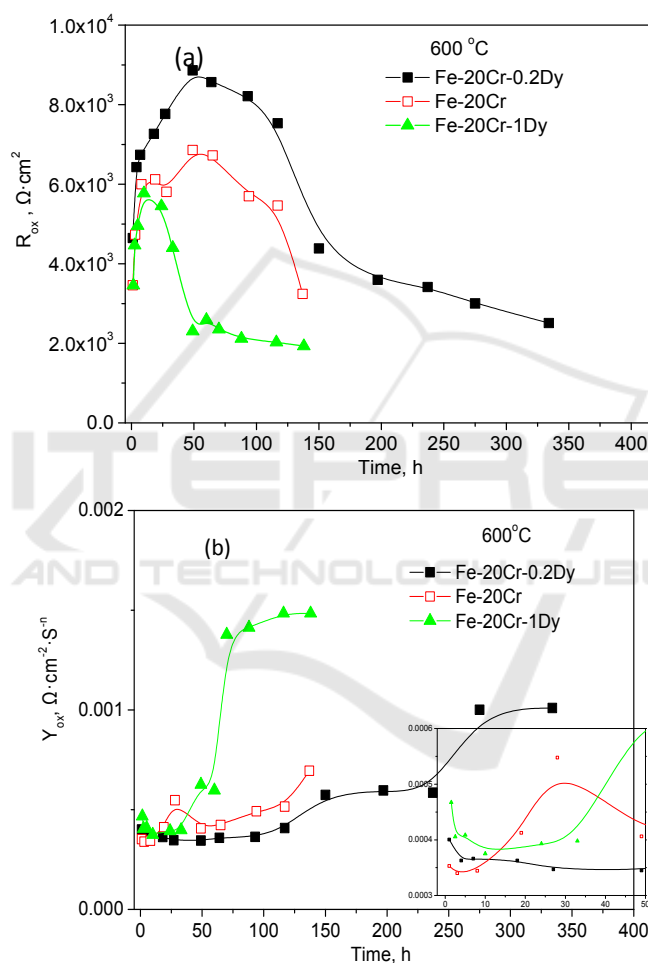**Figure 4.** Equivalent circuits for interpretation of EIS.

Figure 5. Changes of R_{ox} (a) and Y_{ox} (b) with exposure time in K_2SO_4-KCl mixture at 600°C.

In the presence of the solid K_2SO_4-KCl mixture, three alloys undergo a two-stage corrosion behavior during the period of 414 h. In the incubation period, the corrosion of alloys is mainly associated with the formation of some oxides, because the salt between electrodes is in the solid state. In the second period, the double-layer capacitance arises in reaction process. Fitting results of impedance spectra discloses that the incubation period for Fe-20Cr is about 150 h, Fe-20Cr-0.2Dy about 345 h, and Fe-20Cr-1Dy more than 138h. Transfer resistance of ions R_{ox} increases at the beginning and rapidly reaches a peak value, and then decreases to an appropriate range (Figure 5a).

The values of R_{ox} for Fe-20Cr-0.2Dy are the greatest in three alloys. R_{ox} of Fe-20Cr-1Dy is roughly coincident with Fe-20Cr during the period of 24h. However, the values sharply decline after 33h. The results indicate that the protection of oxide scales formed on Fe-20Cr-0.2Dy is better than Fe-20Cr, but that on Fe-20Cr-1Dy is worse than Fe-20Cr, especially for the long exposure duration. The values of oxide capacitance Y_{ox} in Figure 5b show that Y_{ox} gradually increases with time. The values of Fe-20Cr are the larger than other alloys and that of Fe-20Cr-0.2Dy is the smallest. The evolution of Y_{ox} is consistent with transfer resistance of ions through the scale.

3.4. Corrosion mechanism

The corrosion of alloys involves complicated reaction stages including the incubation period and acceleration period. At the initial stage, oxidation occurs at the salt/alloy interface. The increasing of Cr content in Fe-based alloys is beneficial to the formation of protective oxides. Furthermore, the proper addition of Dy could also contribute to the formation of protective oxide scale. In the next reaction process, the K_2SO_4-KCl mixture will readily react with the Fe oxides, Cr oxides and Dy oxides in the oxide/salt interface. At the same time, reactions in the oxide/alloys interface may also occur due to the penetration of K_2SO_4 and KCl through the macro-cracks or pores within the oxide scales. The large amount of chlorine forming will evidently increase chlorine partial pressure and decrease oxygen partial pressure. The gaseous chlorine gradually diffuses into oxide/alloy interface, and directly reacts with alloys to form the solid $FeCl_2$, $CrCl_2$ and $DyCl_2$, respectively. When the partial pressure of chloride is high enough, the gaseous chloride diffuses back into the oxide/salt interface[14]. Fe oxides, Cr oxides and Dy oxides again precipitate on the zone of high oxygen partial pressure. The oxide scale formed by this way is rather porous and can hardly provide any effective protection, so that the corrosion rate is significantly enhanced. The active/oxidation process results show that the external oxide layer is an expanded and layered structure especially for alloys corroded for a long time (Figure 2). Also, the thickness of external oxide layer remarkably increases by this way.

   Furthermore, the sulphate is commonly hard to diffuse through the compact oxides. When the oxide scale is destroyed by chloride, sulphate diffuses into oxide/alloy interface through cracks or pores of the oxide scales and reacts with alloy. Equilibrium partial pressures of solid Cr chlorides are much lower than Fe chlorides to produce the solid Cr_2O_3. The test results show that corrosion resistance of Fe-20Cr-1Dy is poor in K_2SO_4-KCl mixture and the external oxide scales are particularly loose. It is assumed that equilibrium partial pressure of solid Dy chloride is lower than that of Fe/Cr chlorides or the addition of Dy accelerates the volatilization and re-deposition of Fe/Cr chlorides. When Dy-rich phase precipitates at the grain boundary of Fe-Cr alloy, the intergranular oxidation becomes prominent and the penetration depth of internal oxidation front increases.

4. Conclusions

EIS has been utilized to synchronously monitor the corrosion of Fe-20Cr, Fe-20Cr-0.2Dy and Fe-20Cr-1Dy alloys in 0.5K_2SO_4-0.5KCl mixture at 600°C. Corrosion rates of alloys increase with increasing temperature and rise fast with mixed salt partially melting down. Electrochemical parameters calculated from the equivalent circuit discover transfer resistance of ions and charge transfer resistance of Fe-20Cr-0.2Dy are the greatest and followed by Fe-20Cr and Fe-20Cr-1Dy among the three alloys. The detrimental effect of chromium is showed in Fe-20Cr, Fe-20Cr-0.2Dy and Fe-20Cr-1Dy alloys, and corresponding porous and layered corrosion products are showed in cross-section morphology. The addition of Dy accelerates the volatilization and re-deposition of Fe/Cr chlorides.

Acknowledgement

References

[1]   Fukumoto M, Tachikawame C, Matsuzaka Y and Hara M 2012 Corrosion Science **56** 105
[2]   Shinata Y 1987 Oxidation of Metals **27** 315
[3]   Guo P Y, Zhang J Q, Young D J and Konrad C H 2015 Oxidation of metals **83** 223
[4]   He J, Zhang Z, Peng H, Gong S K and Guo H B 2015 Corrosion Science **98** 699
[5]   Lai Y B, Guo P Y, Shao Y, Zhang Y and Liu N 2017 Journal of Alloys and Compounds **694** 383
[6]   Brylewski T, Gil A, Rakowska A, Chevalier S, Adamczyk A, Dabek J, Kruk A, Stygar M and Przybylski K 2013 Oxidation of Metals **80** 83
[7]   Lan H, Yang Z G, Xia Z X, Zhang Y D and Zhang C 2011 Corrosion Science **53** 1476
[8]   Zeng C L, Zhang T, Guo P Y and Wu W T 2004 Corrosion Science **46** 2183
[9]   Liu Z P, Guo P Y and Zeng C L 2007 Journal of Power Sources **166** 348
[10]   Zeng C L, Rizzo F C, Wu WT and Monteiro M J 1999 Corrosion Science **41** 1731
[11]   Zeng C L, Rizzo F C, Monteiro M J and Wu W T 1999 Oxidation of Metals **51** 495
[12]   Guo P Y, Zeng C L, Shao Y and Qin Z S 2012 Journal of Rare Earths **30** 1150
[13]   Zeng C L and Zhang T 2004 Electrochimica Acta **49** 1429
[14]   Zeng C L and Li J 2005 Electrochimica Acta **50** 5533